HHS Public Access

Author manuscript

Abdom Radiol (NY). Author manuscript; available in PMC 2017 September 08.

Published in final edited form as:

Abdom Radiol (NY). 2017 June ; 42(6): 1685–1694. doi:10.1007/s00261-017-1066-y.

Value of Tumor Stiffness Measured with MR Elastography for Assessment of Response of Hepatocellular Carcinoma to Locoregional Therapy

Sonja Gordic, MD[1,2], **Jad Bou Ayache, MD**[3], **Paul Kennedy, PhD**[1], **Cecilia Besa, MD**[1], **Mathilde Wagner, MD, PhD**[1], **Octavia Bane, PhD**[1], **Richard L. Ehman, MD**[4], **Edward Kim, MD**[3], and **Bachir Taouli, MD**[1,3]

[1]Translational and Molecular Imaging Institute, Icahn School of Medicine at Mount Sinai, New York, NY, USA [2]Institute of Diagnostic and Interventional Radiology, University Hospital Zurich, Zurich, Switzerland [3]Department of Radiology, Icahn School of Medicine at Mount Sinai, New York, NY, USA [4]Department of Radiology, Mayo Clinic, Rochester, MN, USA

Abstract

Purpose—To correlate tumor stiffness (TS) measured with MR elastography (MRE) with degree of tumor enhancement and necrosis on contrast-enhanced T1-weighted imaging (CE-T1WI) in hepatocellular carcinomas (HCC) treated with ^{90}Yttrium radioembolization (RE) or transarterial chemoembolization plus radiofrequency ablation (TACE/RFA).

Material and Methods—This retrospective study was IRB-approved and the requirement for informed consent was waived. 52 patients (M/F 38/14, mean age 67 y) with HCC who underwent RE (n=22) or TACE/RFA (n=30) and 11 controls (M/F 6/5, mean age 64 y) with newly diagnosed untreated HCC were included. The MRI protocol included a 2D MRE sequence. TS and LS (liver stiffness) were measured on stiffness maps. Degree of tumor necrosis was assessed on subtraction images by two observers, and tumor enhancement ratios (ER) were calculated on CE-T1WI by one observer.

Results—63 HCCs (mean size 3.2 ± 1.6 cm) were evaluated. TS was significantly lower in treated vs. untreated tumors (3.9 ± 1.8 vs. 6.9 ± 3.4 kPa, p=0.006) and also compared to LS (5.3 ± 2.2 kPa, p=0.002). There were significant correlations between TS and each of enhancement ratios (r=0.514, p=0.0001), and percentage of necrosis (r= -0.540, p=0.0001). The observed correlations were stronger in patients treated with RE (TS vs. ER, r=0.636, TS vs. necrosis, r=

Corresponding Author: Bachir Taouli, MD, Department of Radiology and Translational and Molecular Imaging Institute, Icahn School of Medicine at Mount Sinai, One Gustave L. Levy Place, Box 1234, New York, NY 10029-6574, Tel: (212) 824-8453, Fax: (646) 537-9689, bachir.taouli@mountsinai.org.

Conflict of Interest:

The authors declare that they have no conflict of interest.

COMPLIANCE WITH ETHICAL STANDARDS

Ethical approval: All procedures performed in studies involving human participants were in accordance with the ethical standards of the institutional and/or national research committee and with the 1964 Helsinki declaration and its later amendments or comparable ethical standards.

Informed consent: The Institutional Review Board at our institution approved this single center retrospective study and the need for informed consent was waived.

-0.711, both p=0.0001). Percentage of necrosis and T1-signal in native T1WI were significant independent predictors of TS (p=0.0001 and 0.001, respectively).

Conclusion—TS measured with MRE shows a significant correlation with tumor enhancement and necrosis, especially in HCCs treated with RE.

Keywords

MR Elastography; tumor stiffness; hepatocellular carcinoma; locoregional therapy

Introduction

Hepatocellular carcinoma (HCC) is the most common primary hepatic malignancy and usually develops in the setting of liver cirrhosis. Over the past 20 years, the incidence of HCC in the United States has increased from 1.5 to 4.9 cases per 100,000 individuals, with a concomitant 41% increase in the overall mortality rate [1]. Unfortunately, many patients have advanced-stage disease and are not candidates for radical treatment options such as tumor resection or liver transplantation [2]. In these cases, systemic or loco-regional therapy is used to treat the disease with promising results.

^{90}Yttrium radioembolization (RE), transarterial chemoembolization (TACE), and radiofrequency ablation (RFA) are used as a bridge to liver transplantation, or, for patients with unresectable HCC and have an established palliative role in select patients [3–7]. For patients with small and medium-sized HCC, the combined therapy with TACE/RFA was shown to provide better local tumor control than RFA alone [8–10]. The evaluation of tumor response after loco-regional therapies is essential in directing management of HCC, for repeat treatment and prognosis. Therefore, an accurate imaging method for estimating tumor necrosis is required. Current MRI techniques for assessing HCC treatment response are based primarily on contrast-enhanced T1-weighted imaging (CE-T1WI). Analysis of subtraction images has been shown to provide higher sensitivity and accuracy for the diagnosis of complete tumor necrosis compared with non-subtracted images [11].

MR elastography (MRE) is a phase contrast-based MRI technique for direct visualization and quantitative measurement of propagating mechanical shear waves in biological tissues [12–14]. The technique is used to obtain spatial maps and measurements of shear wave displacement patterns. The wave images are processed to generate maps known as elastograms, which show local quantitative values of the shear modulus of tissues without the need for administration of an exogenous contrast agent [15]. To date, studies have shown that MRE is capable of categorizing liver fibrosis stage [16,17] and differentiating benign and malignant solid liver tumors [18,19]. Recently, the performance of MRE as marker of tumor response was evaluated in two animal studies following chemotherapy. In these studies, reduction in tumor stiffness (TS) was associated with histologically proven central necrosis [20] and decreased cellular proliferation and moderate induction of apoptosis [21]. This suggests that changes in tumor mechanical properties, as changes in interstitial pressures, cellularity, and extracellular components, visualized by MRE may provide early evidence of therapeutic response. Furthermore, MRE enables qualitative and quantitative assessment of tumor stiffness without the use of gadolinium chelates, which makes it a

highly attractive technique, particularly in patients with severe renal dysfunction at risk for nephrogenic systemic fibrosis.

Inspired by these promising results, our aim was to correlate TS measured with MRE with degree of tumor enhancement and necrosis on CE-T1WI and subtraction images in HCCs treated with locoregional therapy.

Material and Methods

Patients

This retrospective study was IRB-approved and the requirement for informed consent was waived. Between July 2013 and September 2015, 160 consecutive patients with HCC undergoing MRI with MRE for evaluation of chronic liver disease were assessed. Diagnosis of HCC was made according to OPTN criteria [22]. 97 patients were excluded from the study for the following reasons: small HCC with a size less than 2 cm not measurable with confidence on MRE (n=22), MRE not covering the index lesion (n=48), HCC not clearly definable on magnitude map (n=12) and image artifacts (n=15). The final study group comprised 63 patients. Diagnosis of liver cirrhosis was based on presence of risk factors and visualization of liver surface nodularity, irregular contour, blunt or rounded edges and/or presence of regenerative nodules. In our study population, all patients had cirrhosis, with the following etiologies: chronic hepatitis C (n=49), chronic hepatitis B (n=13) or cryptogenic cirrhosis (n=1). If there were multiple HCCs present in a patient, only the largest lesion, covered by MRE, was evaluated (Table 1).

MRI and MRE Acquisition

Imaging was performed with different state-of-the-art systems equipped with MRE: 3T GE 750 (n=43), 1.5T GE Signa (n=12) or 1.5 T Siemens Aera (n=8). Routine liver MRI protocol included non-fat suppressed axial and coronal single-shot fast spin-echo T2WI (HASTE/SSFSE), axial fat suppressed fast spin echo (FSE) T2WI, T1WI in- and out-of- phase, diffusion-weighted imaging and dynamic CE-T1WI including subtracted images.

For dynamic CE-T1WI, unenhanced, early (AP1) and late arterial phases (AP2), portal venous phase (PVP) (60s), transitional phase (TP) (180s), and hepatobiliary phase (HBP) (10 and 20 min) were obtained using a 3D T1WI breath-hold fat-suppressed spoiled gradient-recall echo sequence (VIBE or LAVA) before and after administration of gadoxetic acid disodium (Primovist/Eovist, Bayer HealthCare). A fixed dose of 10 ml of contrast (mean weight-based dose of 0.03 mmol/kg) was injected at a rate of 1.5 ml/s followed by a 20 ml saline flush using a bolus tracking technique.

Liver MRE was performed after contrast administration between 10–20 min T1W HBP acquisition [23] using a 2D GRE sequence, with equivalent parameters between systems. For MRE wave generation, a 19-cm-diameter passive acoustic driver was placed on the right side of the abdomen at the level of the xiphoid. Four axial slices were centered over the portal vein using SSFSE axial and coronal sequences for guidance. Wave propagation was captured using a modified phase contrast gradient echo sequence with motion encoding gradient (MEGs) along the slice-select axis. The following sequence parameters were used

for the GE systems: slice thickness 10 mm, matrix 256 × 80, TR/TE 50/20, mechanical motion frequency 60 Hz (power 50%), MEG 60 Hz, ASSET factor of 2, acquisition time 14 seconds/slice (56 seconds); 4 breath-holds with end expiration. For the Siemens system the following parameters were used: slice thickness 7 mm, matrix 256 × 90, TR/TE 50/25, mechanical motion frequency 60 Hz (power 50%), MEG 60 Hz, GRAPPA factor 3, acquisition time 14 seconds/slice (56 seconds); 4 breath-holds with end expiration (Table 2). It has been shown that the reproducibility between platforms is excellent when using 2D GRE [24,25].

The multi-model direct inversion algorithm [15,26], a statistics based direct inversion algorithm, automatically generated stiffness maps from wave images. The confidence index (ranging from 0–100%) for stiffness measurement was estimated using an algorithm reflecting SNR, wave amplitude, multi-path wave interference, and inversion algorithm performance. Stiffness measurements with confidence index >95% were considered reliable.

Qualitative image analysis

Two observers [observer 1, the study coordinator (--), with 2 years of experience in Body MRI; and observer 2 (--) with 5 years of experience in Body MRI] assessed the images in consensus for identification of index tumors. If multiple lesions were present in the same patient, only the largest lesion, covered by MRE, was evaluated. The following features were recorded on conventional sequences (including subtraction) and MRE images: tumor segmental location, maximum tumor size, qualitative enhancement, signal intensity on unenhanced T1WI (iso-, hypo- hyperintense or mixed), degree of tumor necrosis (in 10% increments), quality of wave propagation in the liver and index tumors, and visualization of tumor on magnitude images.

Quantitative image analysis

The study coordinator (--) performed the quantitative analysis 3 to 6 weeks after the initial qualitative image analysis to decrease recall bias. The enhancement ratios (ERs) were calculated using oval or circular regions of interest (ROIs) placed on the whole index tumors, including necrotic portions, on native and CE-T1WI obtained at the second arterial phase (which was selected due to best arterial enhancement of HCCs). Measurements were performed on the largest tumor slice (OsiriX, Bernex, Switzerland).

The ERs were calculated as follows: ER = [SI post – SI pre)/SI pre] × 100%, at AP2.

The stiffness measurements were performed 3 weeks after measurement of the ERs. We assessed the magnitude images obtained with MRE together with native and CE-T1WI. After controlling for variability between sequences due to differences in breathing pattern, ROIs were copied from the native or CE-T1WI to the magnitude map and manually adjusted if the position was slightly different. ROIs were positioned to include most of the index HCC lesions ($6.3 \pm 11.5\ cm^2$). Oval or circular ROIs were also placed in liver parenchyma away from lesions (mean size $4.1 \pm 2.3\ cm^2$) avoiding large vessels. ROIs of HCCs and liver parenchyma were then copied to the stiffness maps and mean stiffness values (tumor stiffness: TS and liver stiffness: LS, in kPa) were measured. The wave propagation was analyzed in every exam. When there was poor wave propagation in the lesion or liver, the

study was excluded. Patients with strong breathing or motion artifacts were also excluded (n=12).

Statistical analysis

Quantitative variables were expressed as mean ± standard deviation and categorical variables as frequencies or percentages. A Kruskal-Wallis H test with Dunn-Bonferroni correction was used to test for significant differences between TS in treated and untreated tumors and LS. A Mann-Whitney U test was used to test for significant differences between patients treated with RE and TACE/RFA, TS in tumors with necrosis < 50% and ≥ 50%, TS in tumors, which were either T1 hyperintense or T1 hypo-, iso- or hypointense with hyperintense rim and TS in tumors imaged ≤ 8 weeks or > 8 weeks after treatment. Pearson correlation was performed between TS and tumor size, TS and percentage of necrosis, and TS and ER. Multiple regression analysis including age, sex, type of treatment, T1 signal and visually assessed percentage of necrosis in the model was performed to test for independent predictors of TS. All statistical analyses were conducted using SPSS software (release 21.0; SPSS, Chicago, Il). A two-tailed p-value less than 0.05 was considered to indicate a significant difference.

Results

The final study group consisted of 63 patients of whom 52 were treated (RE n=22, TACE/RFA n=30), and 11 were untreated (Table 1). In 12 (23%) patients, the diagnosis of HCC was proven on histologic examination, in 40 (77%) patients with liver cirrhosis, the diagnosis of HCC was made on the basis of dynamic contrast-enhanced MRI using OPTN criteria [22]. From the histologically proven HCCs, 1 (8%) was poorly, 5 (42%) moderately, and 6 (50%) were well differentiated.

The median time delay between the last locoregional treatment and imaging was 84 d (range 3–1393 d). In patients treated with RE, the delay between the last treatment and imaging was ≤8 weeks in 12 patients and >8 weeks in 10 patients (median 85 d, range 7–854 d). In patients treated by TACE/RFA, the delay between the last treatment and imaging was ≤8 weeks in 15 patients and >8 weeks in 15 patients (median 56 d, range 3–1393 d) (Table 1).

Qualitative analysis

Patients treated with RE showed 100% necrosis in 15 patients, 80% necrosis in 1 patient, 50% necrosis in 2 patients, 40%, 30%, 20% and 10% necrosis in 1 patient each. Patients treated with TACE/RFA showed 100% necrosis in 27 patients, 90% necrosis in 1 patients and 50% necrosis in two patients. In untreated HCCs, the visual assessment of tumor necrosis revealed 6 patients with 0% necrosis, 2 patients with 10% necrosis, 1 patient with 20% necrosis, 1 patient with 50% necrosis and 1 patient with 60% necrosis. In patients treated with RE, the signal on T1WI was as follows: isointense (n=8), hypointense (n=9), hypointense with hyperintense rim (n=5). In patients treated with TACE/RFA, we observed the following signal intensities: isointense (n=2), hypointense (n=4), hypointense with hyperintense rim (n=8), and hyperintense (n=16).

Quantitative analysis

The mean diameter of tumors was 3.2 ± 1.6 cm (range 2.0 – 9.8 cm). The ER ranged from 0% in completely necrotic tumors to 121% in completely viable tumors. TS in treated tumors was significantly lower compared to untreated tumors (3.9 ± 1.8 vs. 6.9 ± 3.4 kPa, p=0.006), and compared to LS (3.9 ± 1.8 vs. 5.3 ± 2.2 kPa, p=0.002). The TS in untreated tumors was higher compared to LS (6.9 ± 3.4 vs. 5.3 ± 2.2 kPa, p=0.726), though the difference was not significant (Figure 1A, 3 and 4). There was no significant difference in TS of tumors treated by RE and those treated by TACE/RFA (3.8 ± 1.9 vs. 4.3 ± 1.9 kPa, p=0.725) (Table 3). TS in tumors with necrosis < 50% was significantly higher than in those with necrosis ≥ 50% (7.28 ± 3.0 vs. 3.2 ± 1.1 kPa, p <0.0001) (Figure 1B). No significant correlation was found between TS and tumor size (r=0.083, p=0.518). TS of treated hemorrhagic tumors (with a hyperintense signal on T1WI) was significantly higher compared to treated tumors which were iso, hypo- or hypointense with hyperintense rim (4.8 ± 2.0 vs. 3.6 ± 1.7 kPa, p=0.04) (Figure 1C and 5).

A significant correlation was found between TS and visually assessed percentage of necrosis with a moderate negative correlation (r= -0.540, p=0.0001), and between TS and ER with a moderate positive correlation (r= 0.514, p=0.0001) (Figure 2A and B).

When assessing only patients treated with RE (in which none had significant hemorrhage), we observed a strong significant correlation between TS and visually assessed percentage of necrosis (r= -0.711, p=0.0001), and between TS and ER (r= 0.636, p=0.0001) (Figure 2C and D). TS did not differ between patients stratified by delay between treatment and MRI (≤8 w vs. > 8 w, p=0.731).

Multiple regression analysis including age, sex, type of treatment, T1 signal and visually assessed percentage of necrosis in the model showed that visually assessed percentage of necrosis and T1-signal were significant independent predictors of TS (p=0.0001, and 0,001, respectively) whereby sex, age and type of treatment were not (p range 0.360–0.998).

Discussion

The results of our preliminary study showed that treated tumors had significantly lower TS compared to untreated tumors and cirrhotic liver. Furthermore, intra-tumoral hemorrhage was associated with higher TS. TS was significantly correlated with visually assessed percentage of necrosis and ER. These correlations were stronger when assessing only patients treated with RE.

Venkatesh et al. [19] were among the first investigators to report the stiffness of liver tumors with MRE. They reported the stiffness of 12 untreated HCCs (10.3 ± 2.0 kPa) compared to 5.9 ± 2.5 kPa in cirrhotic liver. In our study, the average TS of untreated HCCs was 6.9 ± 3.4 kPa. A potential explanation for the difference in HCC stiffness may be due to different lesion inclusion. Stiffness values of 5.3 ± 2.2 kPa for cirrhotic background liver in our study are in line with the results of Venkatesh et al. In another recent study by Hennedige et al. [27] stiffness values of 55 untreated HCCs were evaluated. Using a similar MRE technique, the authors reported values of 7.7 ± 2.6 kPa, which is in accordance with our results. The

findings in our study however contrast with those of Garteiser et al. [18] who reported lower untreated HCC stiffness values of 2.51 ± 1.01 kPa. The discrepancy in stiffness values may be secondary to a number of factors including the use of a different pulse sequence (2D GRE-MRE in the present study compared to 3D MRE in their study), different inversion algorithm and higher actuation frequency compared to the study of Garteiser et al. (60Hz vs. 50Hz). The frequency dependence of biological tissue results in higher stiffness values at higher actuation [28].

Venkatesh et al. [19] found a non-significant linear correlation between tumor size and stiffness and Hennedige et al. [27] also reported an association between tumor size and stiffness. Our data show no such correlation. In contrast to their studies, where different types of malignant and benign liver tumors were analyzed, we only evaluated HCCs. Partial volume effects can affect the estimates of tumor stiffness, so different lesion size distribution may account for the difference in this respect. In the study of Garteiser et al. [18] no such correlation was performed.

Stiffness of tumors, which showed hyperintense signal on native T1WI and therefore were assumed to be hemorrhagic, was significantly higher compared to non-hemorrhagic tumors. In our study hemorrhagic necrosis was only observed in tumors treated with TACE/RFA (16/30 patients), which was reported previously [29]. In patients treated by RE, minimal signs of hemorrhage were encountered in 5 patients. This different behavior might be explained by the delayed cytotoxic effect on tumor necrosis and shrinkage in tumors treated with RE.

In a recent preclinical study, Pepin et al. [21] assessed MRE derived stiffness as a biomarker for early tumor response to chemotherapy. In their study, tumors were grown in the flank of genetically modified mice by injection of non-Hodgkin’s lymphoma cells. MRE was performed before and after injection of a chemotherapeutic agent or saline. In line with our results, which showed significantly lower TS in treated compared to untreated tumors and a significant correlation between TS and qualitatively and quantitatively assessed necrosis, they observed a significant decrease in TS within 4 days of chemotherapy treatment, while no change was observed in saline-treated tumors. Histological analysis showed decreased levels of cellular proliferation in chemotherapy treated tumors. Another preclinical study by Li et al. [20] evaluated MRE derived stiffness in human colorectal carcinoma cells, which were implanted subcutaneously in the flanks of genetically modified mice. MRE was performed before and 24h after treatment with either the vascular disrupting agent ZD6126 (N-acetylcolchinol-O-phosphate) or vehicle control. No significant changes were observed in the vehicle-treated cohort, however ZD6126 induced a significant decrease in TS and this was associated with histologically confirmed central necrosis. These results are also in good agreement with our work.

These results suggest that change in TS may antecede actual cell death as indicated by histology, and that decreasing cellularity may contribute to the change in tissue mechanical properties [20]. This would potentially allow us to use stiffness as a biomarker of treatment response and also to longitudinally monitor treatment response throughout the course of therapy.

In our study, TS did not differ significantly between patients which were imaged ≤ 8 weeks or > 8 weeks after the last treatment. However, in the group scanned > 8 weeks after the last treatment 23/25 patients (8/10 post RE, 15/15 post TACE/RFA) had 100% necrotic tumors whereas in the group which was scanned ≤ 8 weeks after the last treatment, only 20/27 patients (7/12 post RE, 13/15 post TACE/RFA) showed 100% necrosis. The slightly lower number of 100% necrotic tumors in patients treated with RE and scanned ≤ 8 weeks after the last treatment is in line with the results of Riaz et al. [30]. They evaluated the radiologic-pathologic correlation for HCCs treated by RE and showed that length of time from initial RE to explant pathology predicted the degree of histologic necrosis. In their study, all tumors that had < 50% necrosis were explanted < 3 months from radioembolization. This suggests that a longer period is necessary for the radiation to have its cytotoxic effect on tumor, although tumor size is likely another relevant factor in this effect [3].

Our study has several limitations. First, our study was retrospective and MRE was performed for evaluation of chronic liver disease, so some tumors were captured on only one slice. This may affect the accuracy of measurements. A prospective study will therefore be required to confirm our results. Second, MRE was only available at one time-point and we did not look at serial changes in TS. Third, histological proof was not available for every tumor. However, this limitation is unavoidable, as it is not common practice to obtain histological evidence when imaging criteria for HCC are met. Fourth, this study used an MRE technique in which shear waves were imaged in several axial sections and each section was processed with a 2D inversion algorithm. This technique is often called 2D wavefield MRE and is the standard technique currently available in commercial versions of MRE. Studies have shown that this approach provides a reliable assessment of global liver stiffness, but it is also known that shear wave refraction and other effects can lead to systematic overestimation of stiffness in focal liver lesions, due to a breakdown in the basic assumptions required for 2D wavefield MRE. A more advanced approach, known as 3D wavefield MRE, addresses these errors by acquiring and analyzing a full three-dimensional shear data set. For this reason, when 3D wavefield MRE is available in the future, it will be preferable for evaluating focal liver lesion stiffness. A mitigating factor using the 2D MRE technique is that the tendency to overestimate stiffness applies to all examinations in the data set and therefore the relative differences between groups should be valid. Fifthly, as noted earlier, partial volume effects may affect the measured stiffness values, particularly for smaller lesions.

In conclusion, our study shows that MRE is a feasible technique for quantitative evaluation of mechanical properties of treated HCCs, offering new parameters for tissue characterization with MRI. TS measured with MRE may potentially be used as a marker of HCC treatment response to loco-regional therapy, especially after RE. These results need to be verified in a prospective study.

Acknowledgments

Funding:

NIH R01 Grant EB001981

Sonja Gordic: Swiss National Science Foundation, Fellowship P2ZHP3_161691

References

1. El-Serag HB. Epidemiology of hepatocellular carcinoma in USA. Hepatol Res. 2007; 37(Suppl 2):S88–94. DOI: 10.1111/j.1872-034X.2007.00168.x [PubMed: 17877502]
2. Shields A, Reddy KR. Hepatocellular carcinoma: current treatment strategies. Curr Treat Options Gastroenterol. 2005; 8(6):457–466. [PubMed: 16313863]
3. Kulik LM, Atassi B, van Holsbeeck L, Souman T, Lewandowski RJ, Mulcahy MF, Hunter RD, Nemcek AA Jr, Abecassis MM, Haines KG 3rd, Salem R. Yttrium-90 microspheres (TheraSphere) treatment of unresectable hepatocellular carcinoma: downstaging to resection, RFA and bridge to transplantation. J Surg Oncol. 2006; 94(7):572–586. DOI: 10.1002/jso.20609 [PubMed: 17048240]
4. Lu DS, Yu NC, Raman SS, Limanond P, Lassman C, Murray K, Tong MJ, Amado RG, Busuttil RW. Radiofrequency ablation of hepatocellular carcinoma: treatment success as defined by histologic examination of the explanted liver. Radiology. 2005; 234(3):954–960. DOI: 10.1148/radiol.2343040153 [PubMed: 15681691]
5. Maddala YK, Stadheim L, Andrews JC, Burgart LJ, Rosen CB, Kremers WK, Gores G. Drop-out rates of patients with hepatocellular cancer listed for liver transplantation: outcome with chemoembolization. Liver Transpl. 2004; 10(3):449–455. DOI: 10.1002/lt.20099 [PubMed: 15004776]
6. Bruix J, Sherman M. Practice Guidelines Committee AAftSoLD. Management of hepatocellular carcinoma. Hepatology. 2005; 42(5):1208–1236. DOI: 10.1002/hep.20933 [PubMed: 16250051]
7. Llovet JM, Real MI, Montana X, Planas R, Coll S, Aponte J, Ayuso C, Sala M, Muchart J, Sola R, Rodes J, Bruix J. Barcelona Liver Cancer G. Arterial embolisation or chemoembolisation versus symptomatic treatment in patients with unresectable hepatocellular carcinoma: a randomised controlled trial. Lancet. 2002; 359(9319):1734–1739. DOI: 10.1016/S0140-6736(02)08649-X [PubMed: 12049862]
8. Morimoto M, Numata K, Kondou M, Nozaki A, Morita S, Tanaka K. Midterm outcomes in patients with intermediate-sized hepatocellular carcinoma: a randomized controlled trial for determining the efficacy of radiofrequency ablation combined with transcatheter arterial chemoembolization. Cancer. 2010; 116(23):5452–5460. DOI: 10.1002/cncr.25314 [PubMed: 20672352]
9. Kim JH, Won HJ, Shin YM, Kim SH, Yoon HK, Sung KB, Kim PN. Medium-sized (3.1–5.0 cm) hepatocellular carcinoma: transarterial chemoembolization plus radiofrequency ablation versus radiofrequency ablation alone. Ann Surg Oncol. 2011; 18(6):1624–1629. DOI: 10.1245/s10434-011-1673-8 [PubMed: 21445671]
10. Kim JW, Kim JH, Won HJ, Shin YM, Yoon HK, Sung KB, Kim PN. Hepatocellular carcinomas 2–3 cm in diameter: transarterial chemoembolization plus radiofrequency ablation vs. radiofrequency ablation alone. Eur J Radiol. 2012; 81(3):e189–193. DOI: 10.1016/j.ejrad.2011.01.122 [PubMed: 21353417]
11. Kim S, Mannelli L, Hajdu CH, Babb JS, Clark TW, Hecht EM, Taouli B. Hepatocellular carcinoma: assessment of response to transarterial chemoembolization with image subtraction. J Magn Reson Imaging. 2010; 31(2):348–355. DOI: 10.1002/jmri.22038 [PubMed: 20099348]
12. Ehman RL, Crues JV, Lenkinski RE, Lomas DJ, McVeigh ER, Mitchell DG, Outwater EM, Pettigrew RI, Ross JR. Magnetic resonance. Radiology. 1996; 198(3):920–926. DOI: 10.1148/radiology.198.3.8628896 [PubMed: 8628896]
13. Muthupillai R, Ehman RL. Magnetic resonance elastography. Nat Med. 1996; 2(5):601–603. [PubMed: 8616724]
14. Muthupillai R, Lomas DJ, Rossman PJ, Greenleaf JF, Manduca A, Ehman RL. Magnetic resonance elastography by direct visualization of propagating acoustic strain waves. Science. 1995; 269(5232):1854–1857. [PubMed: 7569924]
15. Manduca A, Oliphant TE, Dresner MA, Mahowald JL, Kruse SA, Amromin E, Felmlee JP, Greenleaf JF, Ehman RL. Magnetic resonance elastography: non-invasive mapping of tissue elasticity. Med Image Anal. 2001; 5(4):237–254. [PubMed: 11731304]

16. Murphy MC, Huston J 3rd, Jack CR Jr, Glaser KJ, Manduca A, Felmlee JP, Ehman RL. Decreased brain stiffness in Alzheimer's disease determined by magnetic resonance elastography. J Magn Reson Imaging. 2011; 34(3):494–498. DOI: 10.1002/jmri.22707 [PubMed: 21751286]
17. Yin M, Talwalkar JA, Glaser KJ, Manduca A, Grimm RC, Rossman PJ, Fidler JL, Ehman RL. Assessment of hepatic fibrosis with magnetic resonance elastography. Clin Gastroenterol Hepatol. 2007; 5(10):1207–1213. e1202. DOI: 10.1016/j.cgh.2007.06.012 [PubMed: 17916548]
18. Garteiser P, Doblas S, Daire JL, Wagner M, Leitao H, Vilgrain V, Sinkus R, Van Beers BE. MR elastography of liver tumours: value of viscoelastic properties for tumour characterisation. Eur Radiol. 2012; 22(10):2169–2177. DOI: 10.1007/s00330-012-2474-6 [PubMed: 22572989]
19. Venkatesh SK, Yin M, Glockner JF, Takahashi N, Araoz PA, Talwalkar JA, Ehman RL. MR elastography of liver tumors: preliminary results. AJR Am J Roentgenol. 2008; 190(6):1534–1540. DOI: 10.2214/AJR.07.3123 [PubMed: 18492904]
20. Li J, Jamin Y, Boult JK, Cummings C, Waterton JC, Ulloa J, Sinkus R, Bamber JC, Robinson SP. Tumour biomechanical response to the vascular disrupting agent ZD6126 in vivo assessed by magnetic resonance elastography. Br J Cancer. 2014; 110(7):1727–1732. DOI: 10.1038/bjc.2014.76 [PubMed: 24569471]
21. Pepin KM, Chen J, Glaser KJ, Mariappan YK, Reuland B, Ziesmer S, Carter R, Ansell SM, Ehman RL, McGee KP. MR elastography derived shear stiffness--a new imaging biomarker for the assessment of early tumor response to chemotherapy. Magn Reson Med. 2014; 71(5):1834–1840. DOI: 10.1002/mrm.24825 [PubMed: 23801372]
22. Wald C, Russo MW, Heimbach JK, Hussain HK, Pomfret EA, Bruix J. New OPTN/UNOS policy for liver transplant allocation: standardization of liver imaging, diagnosis, classification, and reporting of hepatocellular carcinoma. Radiology. 2013; 266(2):376–382. DOI: 10.1148/radiol.12121698 [PubMed: 23362092]
23. Motosugi U, Ichikawa T, Sou H, Sano K, Muhi A, Ehman RL, Araki T. Effects of gadoxetic acid on liver elasticity measurement by using magnetic resonance elastography. Magn Reson Imaging. 2012; 30(1):128–132. DOI: 10.1016/j.mri.2011.08.005 [PubMed: 21937180]
24. Yasar TK, Wagner M, Bane O, Besa C, Babb JS, Kannengiesser S, Fung M, Ehman RL, Taouli B. Interplatform reproducibility of liver and spleen stiffness measured with MR elastography. J Magn Reson Imaging. 2016; 43(5):1064–1072. DOI: 10.1002/jmri.25077 [PubMed: 26469708]
25. Serai SD, Yin M, Wang H, Ehman RL, Podberesky DJ. Cross-vendor validation of liver magnetic resonance elastography. Abdom Imaging. 2015; 40(4):789–794. DOI: 10.1007/s00261-014-0282-y [PubMed: 25476489]
26. Silva AM, Grimm RC, Glaser KJ, Fu Y, Wu T, Ehman RL, Silva AC. Magnetic resonance elastography: evaluation of new inversion algorithm and quantitative analysis method. Abdom Imaging. 2015; 40(4):810–817. DOI: 10.1007/s00261-015-0372-5 [PubMed: 25742725]
27. Hennedige TP, Hallinan JT, Leung FP, Teo LL, Iyer S, Wang G, Chang S, Madhavan KK, Wee A, Venkatesh SK. Comparison of magnetic resonance elastography and diffusion-weighted imaging for differentiating benign and malignant liver lesions. Eur Radiol. 2016; 26(2):398–406. DOI: 10.1007/s00330-015-3835-8 [PubMed: 26032879]
28. Asbach P, Klatt D, Schlosser B, Biermer M, Muche M, Rieger A, Loddenkemper C, Somasundaram R, Berg T, Hamm B, Braun J, Sack I. Viscoelasticity-based staging of hepatic fibrosis with multifrequency MR elastography. Radiology. 2010; 257(1):80–86. DOI: 10.1148/radiol.10092489 [PubMed: 20679447]
29. Kierans AS, Elazzazi M, Braga L, Leonardou P, Gerber DA, Burke C, Qureshi W, Kanematsu M, Semelka RC. Thermoablative treatments for malignant liver lesions: 10-year experience of MRI appearances of treatment response. AJR Am J Roentgenol. 2010; 194(2):523–529. DOI: 10.2214/AJR.09.2621 [PubMed: 20093619]
30. Riaz A, Kulik L, Lewandowski RJ, Ryu RK, Giakoumis Spear G, Mulcahy MF, Abecassis M, Baker T, Gates V, Nayar R, Miller FH, Sato KT, Omary RA, Salem R. Radiologic-pathologic correlation of hepatocellular carcinoma treated with internal radiation using yttrium-90 microspheres. Hepatology. 2009; 49(4):1185–1193. DOI: 10.1002/hep.22747 [PubMed: 19133645]

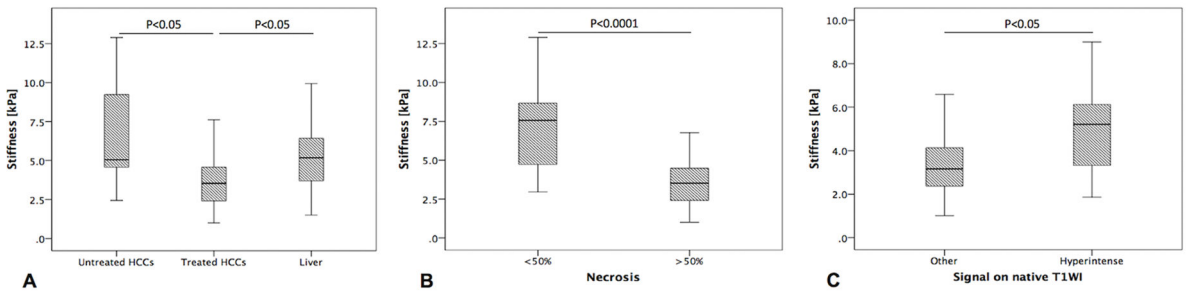

Figure 1.

Boxplots showing measurements of tumor stiffness (TS) in untreated and treated HCCs and background cirrhotic liver (Liver) (A), tumor stiffness (TS) in HCCs with <50% necrosis and ≥50% necrosis (B) and tumor stiffness (TS) in HCCs with either isointense, hypointense or hypointense with hyperintense rim (other) or hyperintense signal on native T1-weighted images (T1WI).

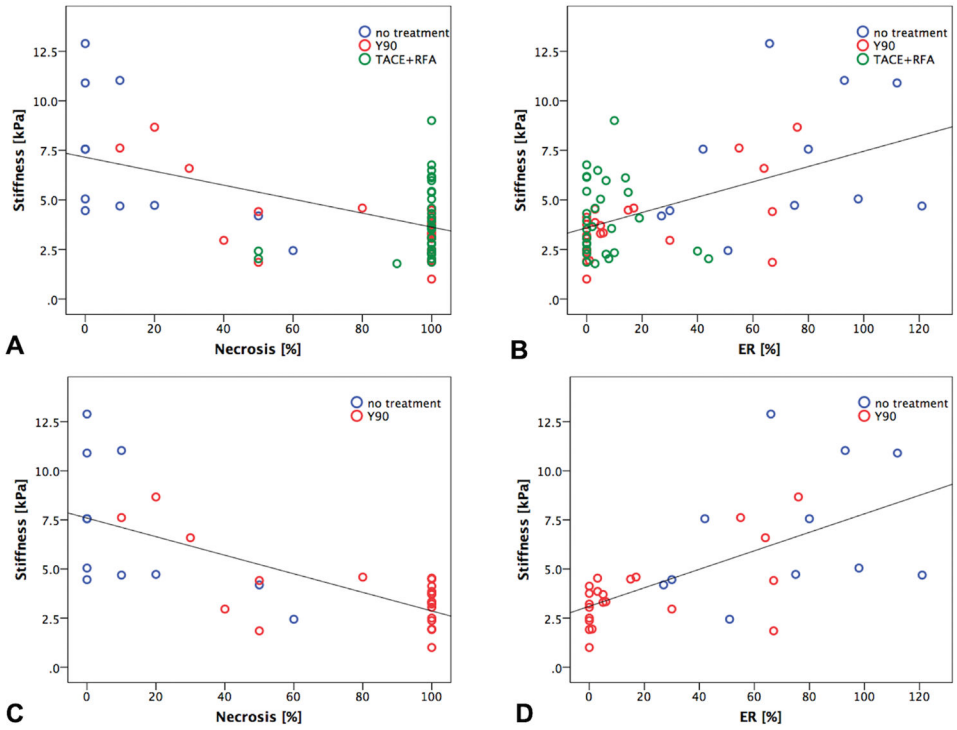

Figure 2.

Scatterplots show Pearson correlation between HCC tumor stiffness values measured with MRE and visually assessed degree of tumor necrosis (r= -0.540, P= 0.0001) (A) and enhancement ratios (r= 0.514, P= 0.0001) (B), respectively. The observed correlations were stronger in the group of patients treated with RE (r= -0.771, P= 0.0001) (C) and (r= 0.636, P= 0.0001) (D), respectively.

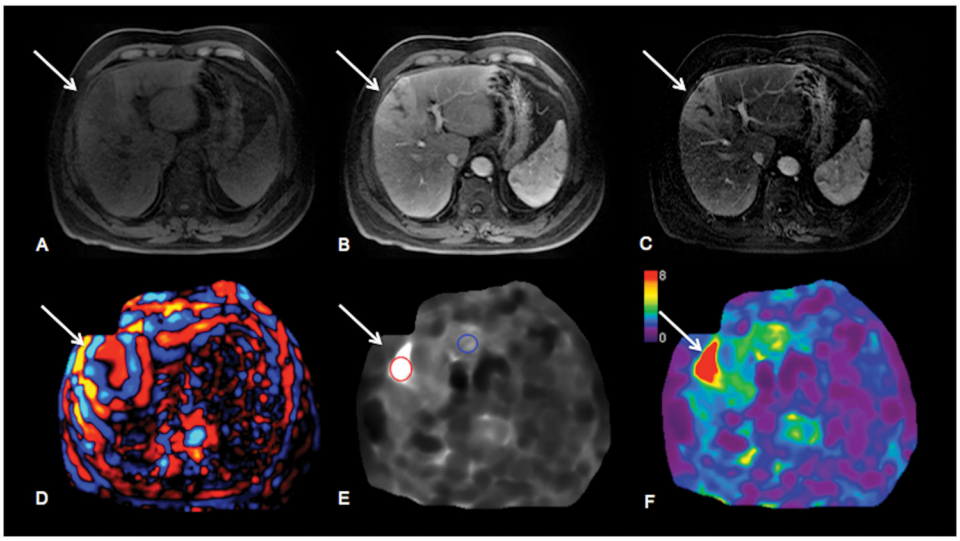

Figure 3.

67-year-old male patient with HCV cirrhosis and untreated infiltrative HCC in left hepatic lobe. HCC (arrows) shows hypointense signal on native T1-weighted images (T1WI) (A) and hyperenhancement on contrast-enhanced T1WI obtained during arterial phase (B). Subtraction images (C) were analyzed for diagnosis of necrosis. Wave image (D) demonstrates excellent wave propagation through the tumor, with longer wavelength in tumor compared to surrounding liver parenchyma. Stiffness map (E) demonstrates visually higher stiffness in HCC vs. liver parenchyma (stiffness values were 11.6 kPa in HCC and 4.0 kPa in liver). HCC is well visualized on elastogram color map (F).

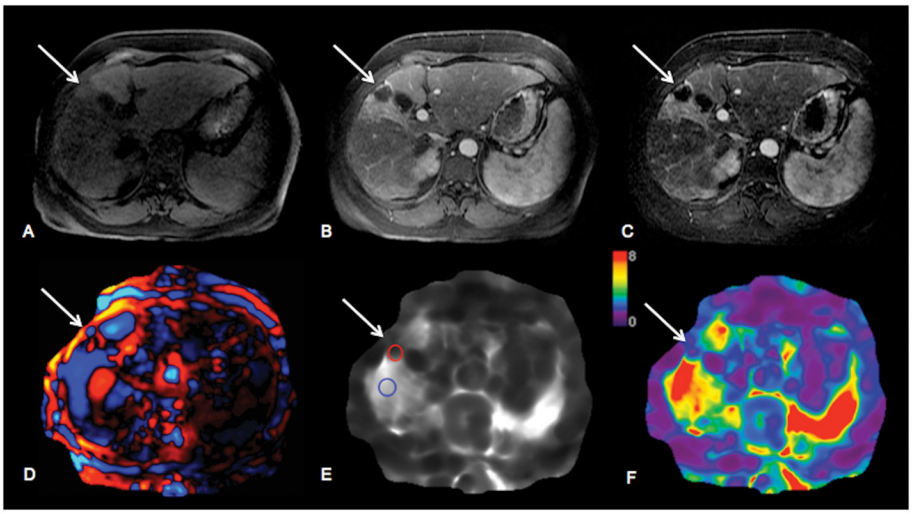

Figure 4.

63-year-old female patient with HCV cirrhosis and HCC in left hepatic lobe (segment 4) treated with ^{90} Yttrium radioembolization. HCC (arrows) shows hypointense signal on native T1-weighted images (T1WI) (A) and no enhancement on contrast-enhanced T1WI in during arterial phase (B). Subtraction image (C) shows 100% necrosis. Wave image (D) demonstrates excellent wave propagation through the tumor, with shorter wavelength in tumor compared to surrounding liver parenchyma. Stiffness map (E) demonstrates visually lower stiffness in HCC vs. liver parenchyma (stiffness values were 2.6 kPa in HCC and 7.4 kPa in liver). Treated HCC is visualized on elastogram color map (F).

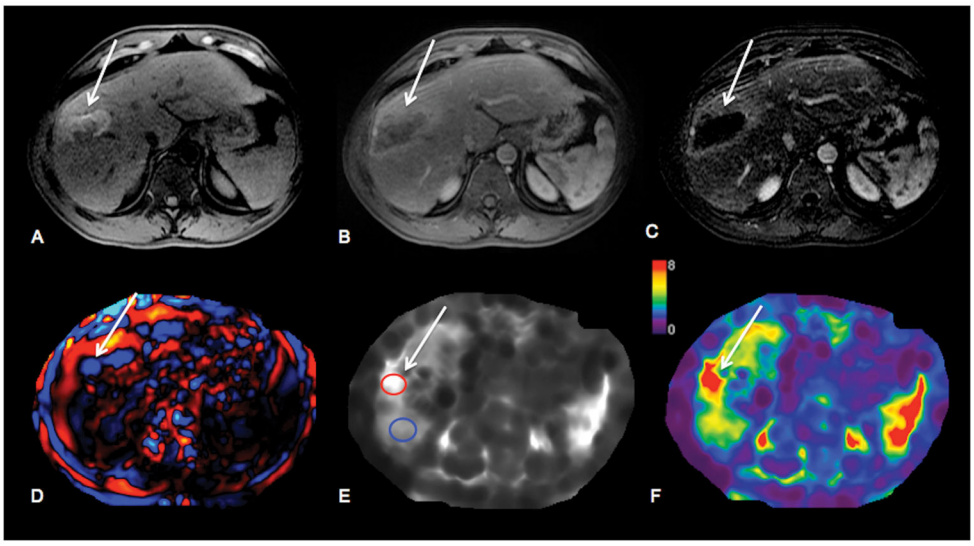

Figure 5.

56-year-old male patient with HCV cirrhosis and HCC in right hepatic lobe treated with transarterial chemoembolization plus radiofrequency ablation. HCC (arrows) shows hyperintense signal on native T1-weighted images (T1WI) (A) compatible with hemorrhagic changes post treatment, and no enhancement on contrast-enhanced T1WI during arterial phase (B). Subtraction image (C) shows complete tumor necrosis. Wave image (D) demonstrates excellent wave propagation through the tumor, with longer wavelength in tumor compared to surrounding liver parenchyma. Stiffness map (E) demonstrates visually higher stiffness in HCC vs. liver parenchyma (stiffness values were 7.3 kPa in HCC and 4.7 kPa in liver). Treated HCC is visualized on elastogram color map (F).

Table 1

Patients' characteristics.

	RE	TACE/RFA	Untreated	p
Number of patients	22	30	11	-
Sex (M/F)	16/6	22/8	6/5	0.734
Age (mean ± SD)	65.5 ± 7.4	68.0 ± 8.2	64.5 ± 7.3	0.186
Liver disease				0.466
Chronic Hepatitis B	2	10	1	
Chronic Hepatitis C	20	19	10	
Cryptogenic	0	1	0	
Median delay between last treatment and imaging (range) [d]	85 (7–854)	56 (3–1393)	-	0.513

Footnote

RE, radioembolization; TACE/RFA, transarterial chemoembolization plus radiofrequency ablation; TS, tumor stiffness

Table 2

Sequence parameters of MRE acquisition.

	GE systems (3T GE 750, 1.5T GE Signa)	Siemens System (1.5 T Siemens Aera)
Slice thickness [mm]	10	7
Matrix	256 × 80	256 × 90
TR/TE	50/20	50/25
Mechanical motion frequency [Hz]	60 (power 50%)	60 (power 50%)
MEG [Hz]	60	60
ASSET/GRAPPA factor	2	3
Acquisition time [sec/slice]	14	14

Footnote

MEG, motion encoding gradient; ASSET, array spatial sensitivity encoding technique; GRAPPA, generalized autocalibrating partially parallel acquisitions

Table 3

Imaging findings.

	RE	TACE/RFA	Untreated	Liver	p
Lesion size (mean ± SD) [cm]	3.2 ± 1.2	3.0 ± 1.4	3.8 ± 2.6	-	0.886
TS/LS (mean ± SD) [kPa]	3.8 ± 1.9	4.3 ± 1.9	6.9 ± 3.4	5.3 ± 2.2	*1***0.002** *2***0.008** *3*0.725 *4***0.004** *5***0.006** *6*0.726

Footnote

*1*RE vs. Untreated;

*2*TACE/RFA vs. Untreated;

*3*RE vs. TACE/RFA;

*4*RE vs. Liver;

*5*TACE/RFA vs. Liver;

*6*Untreated vs. Liver

Significant p-values are bolded

RE, radioembolization; TACE/RFA, transarterial chemoembolization plus radiofrequency ablation; TS, tumor stiffness; LS, liver stiffness